Astron. Astrophys. 324, 1059–1070 (1997)

ASTRONOMY
AND
ASTROPHYSICS

Optical and infrared observations of 23 carbon–rich stars. Modelling of the circumstellar dust shells ⋆

T. Le Bertre

DEMIRM, Observatoire de Paris, 61 av. de l'Observatoire, F-75014 Paris, France

Received 2 December 1996 / Accepted 9 January 1997

Abstract. A study of circumstellar dust shells (CDS) around carbon stars is presented. This study is based on the analysis of the 1–100 μm broad–band spectra of 23 objects which have been monitored in the 1–20 μm region over several years at ESO. The sources in the sample range from Irr/SR variables and optical miras to Extreme Carbon Stars which have only been discovered recently in infrared surveys. A modelling accounting for the photometric variations with phase (with up to 9 spectra per object) has been developed. All the CDSs in the sample can be modelled successfully in spherical geometry with a dust opacity law $\propto \lambda^{-1.3}$ and a dust formation temperature ~ 950 K. The modelling favors the case of an acceleration of dust, from the site of formation and on a distance of $\sim 10^{15}$ cm, over the case of a uniform expansion. Mass loss rates in the range 0.1–50 10^{-6} $M_\odot$ yr^{-1} are derived. The estimates based on this modelling are consistent with those derived from the CO emission line measurements.

In view of the incoming near–infrared surveys (DENIS and 2MASS), an analysis of the location of carbon–rich sources in color diagrams is presented. It is shown that the near–infrared colors are well correlated with the mass loss rate. This property can be used to get an estimate, within a factor 3, of this rate for carbon stars without a priori on the distance.

Key words: radiative transfer – stars: carbon – *(stars:)* circumstellar matter – stars: mass loss – stars: AGB and post–AGB – infrared: stars

1. Introduction

Evolved stars on the Asymptotic Giant Branch (AGB) are known to be surrounded by expanding shells. The infrared excesses of these objects indicate that dust is forming in their environments. The infrared spectra can be divided into two classes which are related to the type of the central stars. The M–type stars show features at 10 and 18 μm which are thought to be the signature of amorphous silicate grains (Day 1974). On the other hand, the C–type stars display a feature at 11.3 μm ascribed to silicon carbide (SiC, Treffers & Cohen 1974). This differentiation is believed to be due to the chemistry of the central star photospheres and to the great stability of the CO molecule. In M–type stars, the abundance of oxygen is larger than the one of carbon (C/O < 1), so that all carbon is locked into CO. This situation is favorable to the formation of silicate compounds (Salpeter 1974). In C–type stars, the reverse situation applies and one expects the formation of carbon–rich particles. In both cases, once dust is formed, it is submitted to radiation pressure and accelerated outwards dragging with it the gas (Kwok 1975). Therefore, although it is a minute component in the circumstellar media (≤ 1.5 % in mass for cosmic abundances), dust appears as the cause of their expansion, and hence of mass loss from evolved stars.

The circumstances accompanying the dust formation are not well understood. Although stationary models of expanding shells can be built (Dominik et al. 1990), mass loss seems more or less correlated to stellar period (DeGioia–Eastwood et al. 1981, Jura 1986). Therefore it is likely that the stellar variability favors the formation of grains around evolved stars. Recently, models of dust formation induced by stellar pulsations have been built (Fleischer et al. 1992) and they have been shown to be successful in reproducing some of the features seen in long–period variable light curves (Winters et al. 1994b).

In this context, it appears that a study of the variability of evolved stars in the infrared might give insights on the processes of dust formation and mass loss. With this motivation, a monitoring programme was undertaken at the ESO 1–m telescope. The results for the oxygen–rich sources have been reported by Le Sidaner & Le Bertre (1996). In the present paper, we report a similar study directed to the carbon–rich sources. The sample of sources is presented in Sect. 2 together with the observational results relevant to our study. A model used to interpret the infrared data is presented in Sect. 3 and the results of its application to the sources belonging to our sample, in Sect. 4. Finally, these results are discussed in Sect. 5.

Send offprint requests to: T. Le Bertre

Tables 2, 3 and 4 are only available in electronic form at the CDS via anonymous ftp 130.79.128.5.

⋆ Based on observations obtained at ESO, La Silla, Chile.

2. Basic data

2.1. Carbon stars

The sample of carbon stars is the same one as in Le Bertre (1992, Paper I). The 23 objects in this sample have been monitored for several years in the near–infrared range (1–5 μm). Most of them (19) have been found to be periodic with periods in the range 350–750 days. Also, all have been observed by IRAS (IRAS Science Team, 1988). The list of sources with their IRAS identifiers are given in Table 1. The periods and the spectral classes are taken from Paper I.

The circumstellar gas expansion velocities, V_{exp} (Table 1), are estimated from half the width at zero level of the CO millimeter emission lines. The values were taken from the catalogue of Loup et al. (1993). When several values are quoted, the average from the best CO (1–0) measurements was adopted. For IRSV 1519–5115, the CO profiles are contaminated by interstellar emission (Nyman et al. 1993). We adopted the value of 22.2 km s^{-1} given by Nyman et al. In the case of AFGL 971, V_{exp} is uncertain (Zuckerman & Dyck 1986).

The distances were derived from the periods and from the averages over time of the bolometric luminosities, obtained from the 1–100 μm energy distributions (Sect. 4), by using the Period–Luminosity relation for carbon stars of Groenewegen & Whitelock (1996) and adopting a distance modulus for the LMC of 18.5:

$$M_{bol} = -2.59 \log P + 2.02.$$

For IRC –30060, "CRL 1047"[1] and IRSV 1301–6242, as there is no period, arbitrary distances of respectively 1, 3 and 3 kpc, have been adopted. They led to "reasonable" luminosities ($\sim 5\,10^3$ L$_\odot$, see Table 4).

2.2. Broad–band energy distributions

Photometric data in the range 1–20 μm have been obtained from 1984 to 1990 with the ESO 1–m telescope. The 1–5 μm results (J, H, K, L', M) have been reported in Paper I. The density of measurements (up to 32 epochs) allowed the derivation of periods, phases and average parameters of the light curves. On the other hand, the 8–20 μm observations (N, N1, N2, N3, Q0) were performed less regularly (up to 9 epochs). Nevertheless, care was taken to acquire them within $\pm$ 1 day of the near–infrared measurements (with the exception of 2 cases discussed in Sect. 2.3). The data are given in Table 2. The data on AFGL 3068 have already been published in Le Bertre et al. (1995, Paper II) and are not reported in this Table.

The corresponding sets of data have been used to derive the 1–20 μm energy distributions of the sources at the epochs given in Table 2. A few examples of the 79 resulting spectra are shown in Fig. 1 and following; others can be found in Le Bertre (1987, 1988a, 1988b, 1990) where preliminary results from this programme have been presented. By fitting a blackbody curve to these spectra, an estimation of the color temperature, T_{BB}, has been obtained for each source. The values are reported in Table 1.

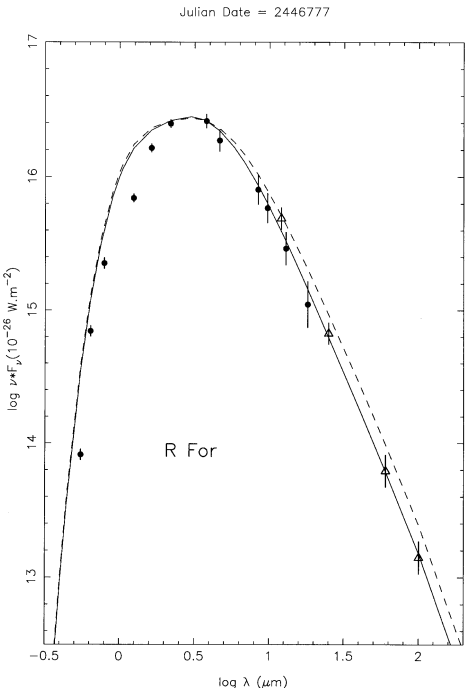

Fig. 1. Energy distribution of R For. The dots represent data obtained at the ESO 1-m telescope (infrared data: JD=2446779; optical data: JD=2446777) and the triangles, IRAS data. The dashed line corresponds to a fit with a $\propto r^{-2}$ dust density distribution and the solid line, to a fit with a density profile given by the Schutte & Tielens (1989, ST) approximation (Sect. 4.1). For both fits, the optical depth is the same, $\tau_{1\mu m} = 1.0$. The fits are almost identical in the NIR range, but differ at longer wavelengths

All sources were detected by IRAS (IRAS Science Team, 1988). The flux measurements have been corrected using the color temperatures (T_{BB}) given in Table 1 and the prescriptions of the IRAS Explanatory Supplement. IRAS data are displayed as triangles in Fig. 1 and following. The IRAS observations have been performed through 1983 well before our 1–20 μm observations. For carbon–rich sources, the amplitudes of the light curves decrease rapidly with wavelength (e.g. Fig. 7 in Paper I). Except for the reddest sources (AFGL 865, 3068, 3099), the variations are expected to be small (less than a factor 2 at 12 μm and probably less beyond) so that neglecting the phase should have little consequence.

In addition, for several sources, UBVRI data have been obtained at the ESO 1–m telescope (Table 3). We have used also these data to complement in some cases the 1–100 μm broad–band spectra (e.g. Fig. 1).

2.3. Comments on individual sources

Some comments about the carbon stars of the sample have already been made in Paper I.

[1] "CRL 1047" is a carbon star discovered by Allen et al. (1977) at the location of an AFGL source (n° 1047) but unrelated to it

Table 1. Fundamental data

name	IRAS name	T_{BB} (K)	V_{exp} km s^{-1}	P days	Spectral class	distance parsec
R Scl	01246–3248	800	17.3	386	C6,5e/C6II	330
R For	02270–2619	1300	20.1	385	C4,3e	540
R Lep	04573–1452	1600	18.7	433	C7,6e/C6IIe	310
AFGL 799	05377+1346	1000		372	C8,4	1830
AFGL 865	06012+0726	500	16.0	696		1500
IRC –30060	06216–2702	1600			C4,4	1000
AFGL 935	06230–0930	800	13.7	494		2240
AFGL 971	06342+0328	650	9.0	653		1420
"CRL 1047"	06563–1905	1800				3000
AFGL 1062	07028–1456	800		582		2080
AFGL 1085	07098–2012	800	23.8	725		1790
IRC –20131	07270–1921	1200	25.5			1300[1]
AFGL 1235	08088–3243	800	20.7	571		1260
IRC +10216	09452+1330	550	15.0	649	C9,5	135
IRAS 11514–5841	11514–5841	500		599		4500
IRSV 1204–6417	12043–6417	800		650		5000
IRSV 1301–6242	13019–6242	1800				3000
IRSV 1519–5115	15194–5115	700	22.2	580		540
IRC +10401	19008+0726	800	18.2	577		1010
IRC –10502	19175–0807	800	31.8	676	C5,4	840
AFGL 2392	19248+0658	1000		493	C7,3	2000
AFGL 3068	23166+1655	300	14.0	696		1140
AFGL 3099	23257+1038	500	10.1	484		1500

[1]: see Sect. 2.3

• R Scl: an excess in the IRAS fluxes at 60 and 100 μm has been reported by Rowan–Robinson et al. (1986). We adopted $T_{BB} = 800$ K.

• R For: this carbon mira was discussed by Feast et al. (1984) and by Le Bertre (1988a). It was shown that the increased obscuration of the central star around the minimum of bolometric luminosity could be understood by the condensation of dust grains in the inner part of the circumstellar shell.

The light curves of R For have been analyzed in details by Barthès et al. (1996). They find up to 11 components in the Fourier spectrum. All are related to frequencies close to subharmonics of the dominant mode or to linear combinations of them with the latter. Therefore, we sticked to the main period, i.e. 385 days.

• IRC –30060 (CS 1263): the source is variable but without periodicity (Paper I). The variability is clearly detected in the optical range except in U. Also, the U–B index is too small for a carbon star for which it would be expected to be ≥ 3. These two facts point towards the presence of a nearby companion dominating the flux measurements in U.

• AFGL 971: this infrared source has already been discussed in Le Bertre (1988b, Paper III). The star was shown to be located behind a molecular cloud producing an extinction, $A_V \sim 3.1 \pm 0.8$ (Fig. 6).

The 8–20 μm data obtained at epoch 2446222 have no 1–5 μm correspondents within $\pm$ 1 day. They have been merged with the 1–5 μm data obtained at 2446203. The difference in epoch corresponds to 3% of the period (653 days). Nevertheless, as the phase is ~ 0.22, the resulting spectrum should be handled with care.

• IRC –20131 (CS 1732): this carbon star was studied in details by Le Bertre (1990). From an excess in U it was found to have an A–type companion (Fig. 9). A kinematic distance of 1.3 kpc was estimated.

The 8–20 μm data at epoch 2446223 have been merged with the 1–5 μm data at 2446207. The star is an irregular variable and the amplitudes of its variations are relatively small (~ 0.25 mag. at 10 μm).

• AFGL 1085: this source is the carbon star with longest known period (P $\sim$ 725 days). Its light curve clearly shows intermediate extrema on its rising branch (Paper I).

• AFGL 1235: preliminary results have already been presented in Paper III.

• IRC +10216 (CW Leo): this source is the prototype of Extreme Carbon Stars (ECS), i.e. carbon stars surrounded by very dense circumstellar shells. Preliminary results of our programme have already been discussed in Le Bertre (1987) and in Paper III. A model of this source which fits well our data at maximum has also been obtained by Winters et al. (1994a).

• IRAS 11514–5841 (CS 3124): the JHK data are contaminated by a neighbour star of early type (A or F, Paper I) and have not been used.

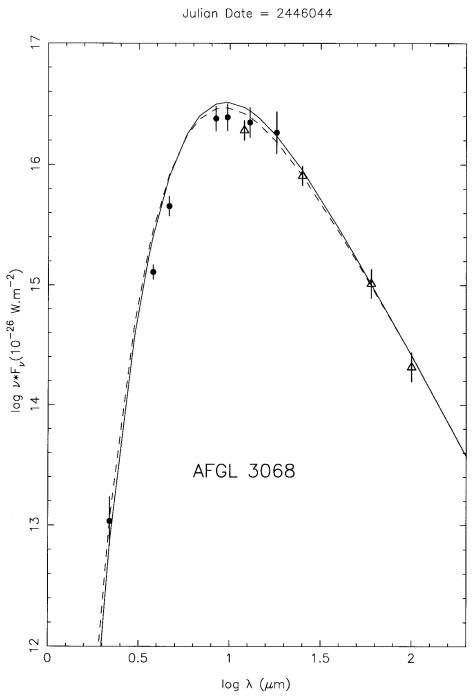

Fig. 2. Energy distribution of AFGL 3068. The dots represent data obtained at the ESO 1-m telescope (JD=2446044) and the triangles, IRAS data. The dashed line corresponds to a fit with a $\propto r^{-2}$ dust density distribution ($\tau_{1\mu m} = 28$) and the solid line, to a fit with a density profile given by the ST approximation ($\tau_{1\mu m} = 36$). Although the optical depths are different, the fits are basically identical

• IRSV 1519–5115: the molecular cloud responsible for the contamination of the CO lines (Sect. 2.1) is at 2.9 kpc (Nyman et al. 1987) and should be behind the AGB star located at ~ 0.5 kpc (Table 1). Therefore, in the interpretation of photometric data, it is probably not necessary to consider interstellar extinction. The same spectrum (Fig. 10) has been modelled successfully by Lopez et al. (1993).
• AFGL 3068: this source is one of the most extreme ECS and is discussed in Paper II. A detailed self–consistent time–dependent model for this source has recently been developed by Winters et al. (1997).
• AFGL 3099 (IZ Peg): Whitelock et al. (1994) report a monitoring in bands H, K and L over 13 years. They find that the data can be fitted by the sum of 2 sine waves with periods of 488 and 345 days. The main component (488 days) agrees with the one obtained in Paper I.

3. Description of the model

To interpret the infrared photometry presented in Sect. 2 we use the model developed in Le Bertre et al. (1995, Paper II) for AFGL 3068 and extend it to the whole sample. The circumstellar dust shells (CDS) are assumed to be spherical with dust condensing at an inner radius R_c. They are supposed to extend outwards to an external limit taken to be at 10 000 R_c. The dust is assumed to be in radiative equilibrium and the transfer of radiation is solved numerically using the method of Leung (1976). Two cases of density distribution have been considered: (i) a density law $\propto 1/r^2$, (ii) a law, $\propto 1/(x - y_0)^{1/2}\, x^{3/2}$, where x is r/R_c, derived by Schutte & Tielens (1989) and approximating the density distribution computed by Tielens (1983). These 2 cases are discussed in more details in Sect. 4.1.

The central stars are assumed to radiate as blackbodies at temperature $T_\star$. It is generally admitted that the first index of the spectral class is an indicator of the carbon star effective temperature. For instance, Cohen (1979) gives 2900 K for a C4 star, 2620 K for a C6 and 2230 K for a C9. However, Ohnaka & Tsuji (1996) claim that this index is poorly correlated with the effective temperature derived by the InfraRed Flux (IRF) method. They suspect that it depends also on the stellar C/O ratio. Even with the IRF method, the uncertainties stay large (~ 150 K). For R Scl (C6,5), they estimate $T_{\rm eff} \sim 2830$ K. Due to the presence of strong molecular bands in the optical range, the stellar effective temperature tends to overestimate $T_\star$. We have adopted $T_\star \sim 2600$ K for R Scl, as well as for the 2 other optical miras (R For and R Lep), for IRC –30060 and for "CRL 1047". For the other objects in the sample, we have adopted $T_\star \sim 2200$ K which seems typical for high–mass–loss carbon stars (Cohen 1979). This corresponds also to the lowest effective temperature considered by Ohnaka & Tsuji. For simplicity, the variation of $T_\star$ with phase has not been considered.

Carbon stars with CDS show in their spectra a feature at 11.3 μm ascribed to silicon carbide (SiC). Some sources (ECS) show also a broad feature at 30 μm which has been attributed to magnesium sulfide (MgS, Goebel & Moseley 1985, Begemann et al. 1994). The 11.3 μm feature is contributing little to the broad band spectrum, but the 30 μm one might contribute to $\sim 30\,\%$ of the fluxes in the IRAS 25 μm band. Apart from these two features the spectra are dominated by featureless continua. The responsible agent has not yet been identified with certainty, but it is likely to be a kind of hydrogeneous amorphous carbon–rich dust. To represent the wavelength dependence of the opacity in carbon–rich sources, Jura (1983) has proposed a law in $\lambda^{-1.3}$ on the basis of infrared and radio observations of IRC +10216. The validity of this law has been checked by us on several sources such as IRC +10216, R For, AFGL 971 and AFGL 1235 (Paper III and references therein). More recently, in Paper II, we have checked that Jura's law applies also to the most extreme ECS, AFGL 3068, for which it was shown to give a good representation of the energy distribution up to ~ 500 μm. It was not possible to conclude on its validity beyond 500 μm because of the contamination of sub–millimeter fluxes by circumstellar molecular emission (Groesbeck et al. 1994). In the following we adopt the same law for all the sources in the sample.

For a given density distribution, the dust density is defined by the optical depth at 1 μm, $\tau_{1\mu m}$. Following the approach of Paper II, the product $\tau_{1\mu m} \times R_c$ is taken to be constant for each object independently of the phase of the central star. This condition expresses that the determination of the dust mass loss rate should be phase–independent (Le Bertre 1988a, Le Sidaner & Le Bertre 1993). Furthermore, the temperature of the dust

grains in R_c, T_c, is also taken to be constant for each object, and we adopt the same value, $T_c \sim 950$ K, for the whole sample. This condition expresses that the same kind of dust should be formed around all carbon stars. Values of T_c outside the range 900–1000 K are excluded for this kind of modelling (see e.g. Papers II and III). As discussed in Paper II, T_c may not represent the condensation temperature of dust nuclei, but rather the accretion temperature of a mantle on these nuclei. In practice, the two conditions, $\tau_{1\mu m} \times R_c \sim$ constant and $T_c \sim 950$ K, are extremely constraining and only one parameter ($\tau_{1\mu m} \times R_c$) can be adjusted for each object independently of the number of spectral energy distributions to be fitted (up to 9 in some cases).

This method relies certainly on too simplistic approximations, for instance the spherical geometry of CDSs or the analytical representation of the opacity. Also, it does not take into account the complexity of dust formation in the atmospheres of carbon stars, nor the dynamics inside CDSs. It is worth noting that the dynamics must be strongly coupled to the stellar variability (Fleischer et al. 1992). In addition, the real carbon stars may have different chemical compositions and one could imagine that the properties of dust differ from object to object. Nevertheless, our global approach allows to study the whole population of carbon–rich sources. Also, elaborate models are difficult to apply massively to a large sample of objects. Finally, it is encouraging to see that, despite all its imperfections, the method works rather satisfactorily to reproduce the observed (1–100 μm) broad band energy distributions of several sources with widely different optical depths (Le Bertre 1988a, Papers II and III).

4. The modelling

4.1. The dust density distribution

Two laws representing the dust density distribution have been examined. First, a law $\propto r^{-2}$ was considered as in previous models (Paper I, etc.). This law expresses that the dust is flowing at a uniform velocity from the inner edge of the CDS and that the mass loss rate is constant. Second, a law $\propto 1/(x - y_0)^{1/2}\, x^{3/2}$, where x is r/R_c and $y_0 = 0.96$ (Schutte & Tielens 1989, hereafter ST), was considered. This law is an analytical approximation of the results of a model of dust dynamics developed by Tielens (1983). Due to the combined actions of radiation pressure and of gas friction, dust is accelerated from R_c outwards and, at $\sim 3 \times R_c$, reaches a uniform velocity. With such a law the distribution is more peaked at the inner boundary than with a law $\propto r^{-2}$, but for $r \gg R_c$ it is in r^{-2}. For the same optical depth, the density in R_c is 3 times the one given by the $\propto r^{-2}$ law and, for $r \gg R_c$, it is 0.6 times the other one. The ST approximation has been used by Le Sidaner & Le Bertre (1993) to model oxygen–rich sources. Due to the larger dust density at the inner boundary, the back warming effect is more important than with a $\propto r^{-2}$ law so that, for the same values of the optical depth and of the inner boundary, R_c, the resulting temperature T_c is larger.

The calculations that have been carried out allow good fits of the spectral energy distributions in both cases. However, some differences are noted. In the case of moderate optical depth ($\tau_{1\mu m} \leq 1$), the temperature T_c is only slightly increased with the ST approximation, e.g. from 950 K to 952 K, all other parameters being kept identical. The emergent spectrum is almost unchanged in the optical range and in the near infrared. At longer wavelengths, the spectrum with the ST approximation falls off below the spectrum obtained with the $\propto r^{-2}$ law (Fig. 1). This can be easily understood as, far away from the central star, the ST density is 0.6 times the one given by the $\propto r^{-2}$ law.

In the case of a large optical depth (e.g. $\tau_{1\mu m} = 34$), T_c is increased from 951 to 973 K, all other parameters being kept identical. In such a case, it is necessary to increase the value of R_c by a factor 1.05 to maintain $T_c = 951$ K. For such large optical depth, the emergent spectrum is mainly coming from the dust at a distance of a few R_c. Therefore, to fit the same spectrum, the optical depth with the ST approximation must be larger than with the $\propto r^{-2}$ law (e.g. Fig. 2).

The examination of the spectra for objects with moderate optical depth such as R For shows that better fits can be obtained with the ST approximation than with the $\propto r^{-2}$ law. The fits for objects with large optical depth can be equally good for both density distributions, but lead to different values of $\tau_{1\mu m}$. The discrimination between the 2 laws obviously must be done on the basis of objects with moderate optical depth for which the emergent spectra contain information on the inner parts of the dust shells. The fact that better fits are obtained for these sources with the ST law confirms that dust is accelerated from R_c on a distance of a few R_c, and shows that this effect must be accounted for in the modelling. Therefore, in the following, we have adopted the ST approximation for all cases.

4.2. Results of the modelling

Several representative fits to the observed energy distributions are shown as solid lines in Fig. 3 and following. As discussed in the previous section, the Schutte & Tielens (1989, ST) approximation has been finally adopted in all cases for representing the dust density distribution. In examining the fits, one should keep in mind that, for carbon stars, the J-band is generally depressed by absorption due to the C_2 and CN band systems. The I and H-bands are also affected by CN. CN and CO are important on the sides of the 2 μm atmospheric window, but do not affect strongly the photometric K-band. The same comment applies to the L'-band, whose bandwidth extends from 3.5 to 4.1 μm and which is not affected by the C_2 and HCN absorption centered at 3.1 μm. Finally, the B-band is strongly affected by C_2. The photometric data in K and L give certainly the best estimation for the source continuum.

The results of the modelling are given in Table 4 for each object at each epoch. The phases, ϕ, are estimated from the periods and epochs of maxima derived in Paper I. The dust shell inner radius, R_c, and the stellar luminosity, $L_\star$, are given for the distances adopted in Table 1. For these distances, R_c is found to be on the order of 10^{14} cm. The temperature T_c has been selected to be ~ 955 K for all sources at all phases (Sect. 3). The exact values resulting from the radiative equilibrium are given

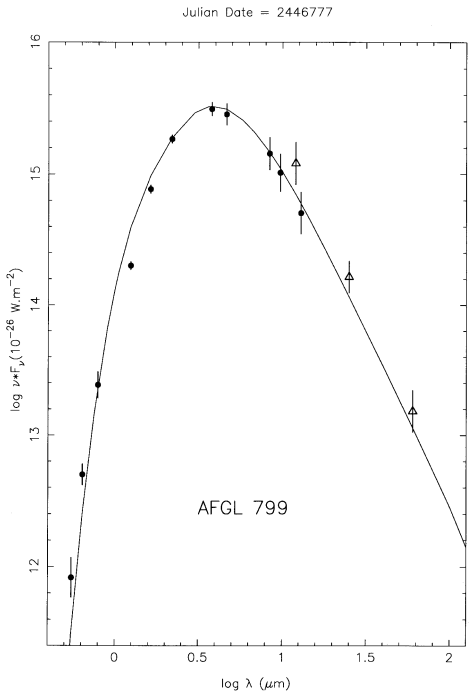

Fig. 3. Energy distribution of AFGL 799. The dots represent data obtained at the ESO 1-m telescope (infrared data: JD=2446781; optical data: JD=2446777) and the triangles, IRAS data. The solid line corresponds to a fit with a density given by the ST approximation ($\tau_{1\mu m} = 2.6$; see Table 4)

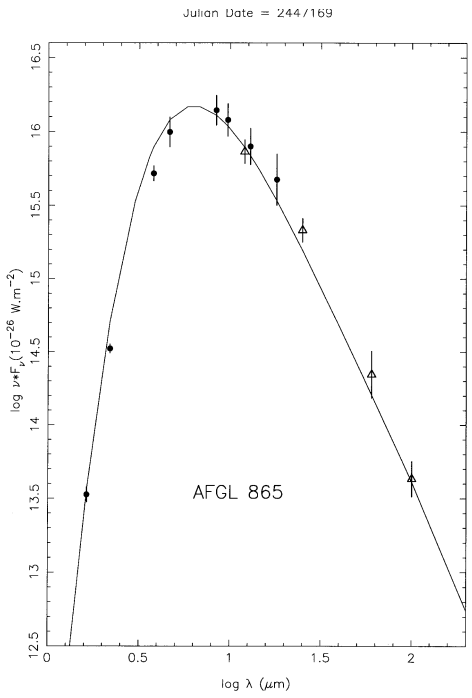

Fig. 4. Same as Fig. 3 for AFGL 865 (infrared data: JD = 2447169; $\tau_{1\mu m} = 12.0$)

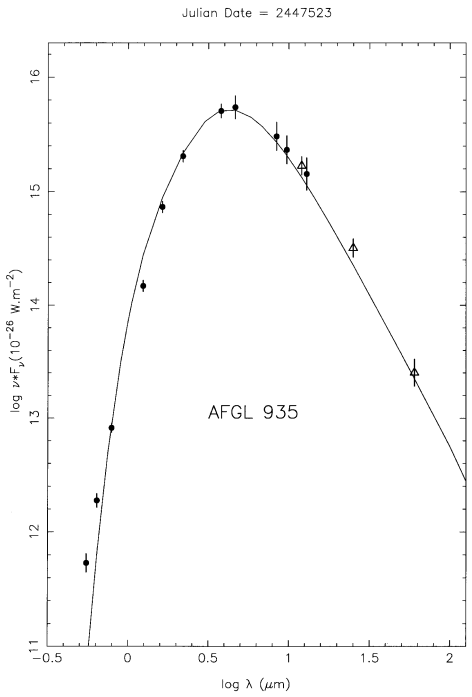

Fig. 5. Same as Fig. 3 for AFGL 935 (infrared data: JD = 2447521; optical data: JD = 2447523; $\tau_{1\mu m} = 3.6$)

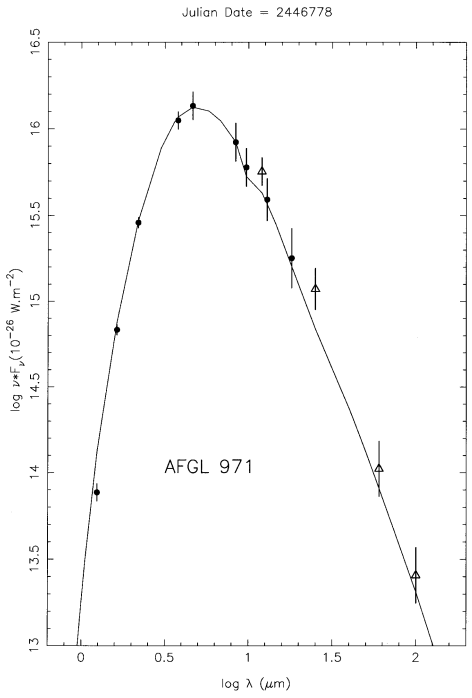

Fig. 6. Same as Fig. 3 for AFGL 971 (infrared data: JD = 2446778; $\tau_{1\mu m} = 5.2$). The model spectrum has been corrected for an interstellar extinction, $A_V = 3.1$ (see Sect. 2.3)

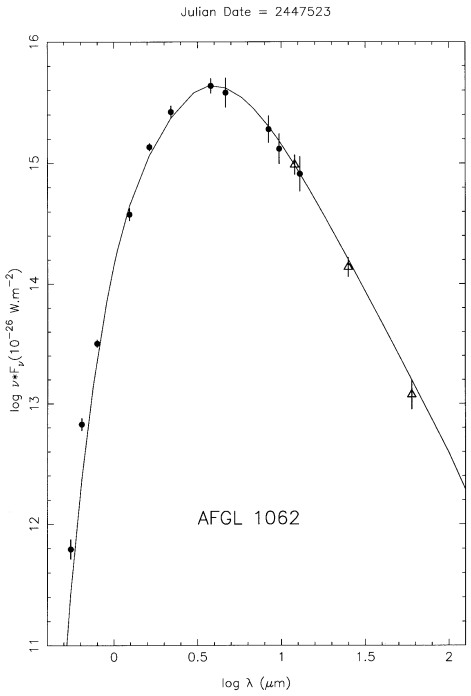

Fig. 7. Same as Fig. 3 for AFGL 1062 (infrared data: JD = 2447521; optical data: JD = 2447523; $\tau_{1\mu m} = 2.8$)

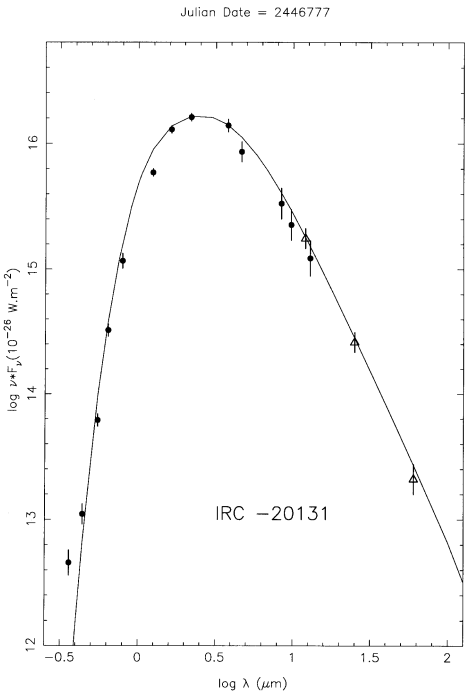

Fig. 9. Same as Fig. 3 for IRC –20131 (infrared data: JD = 2446778; optical data: JD = 2446777; $\tau_{1\mu m} = 0.8$)

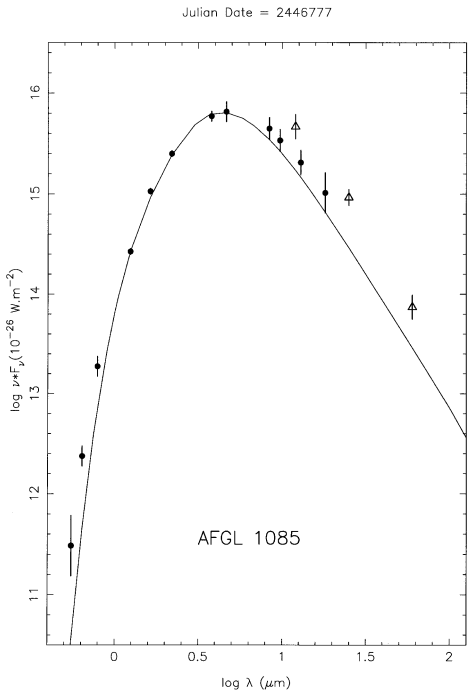

Fig. 8. Same as Fig. 3 for AFGL 1085 (infrared data: JD = 2446778; optical data: JD = 2446777; $\tau_{1\mu m} = 3.9$)

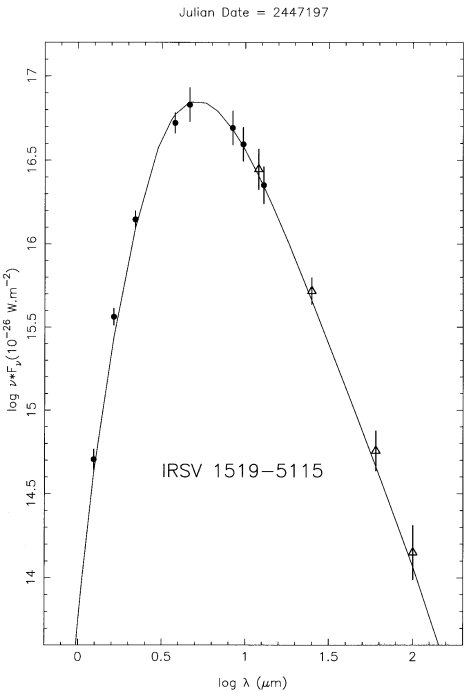

Fig. 10. Same as Fig. 3 for IRSV 1519–5115 (infrared data: JD = 2447197; $\tau_{1\mu m} = 6.4$)

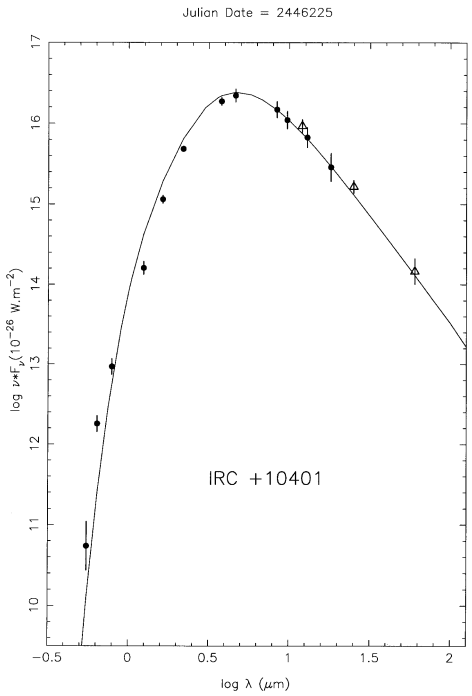

Fig. 11. Same as Fig. 3 for IRC +10401 (infrared data: JD = 2446220; optical data: JD = 2446225; $\tau_{1\mu m} = 5.0$)

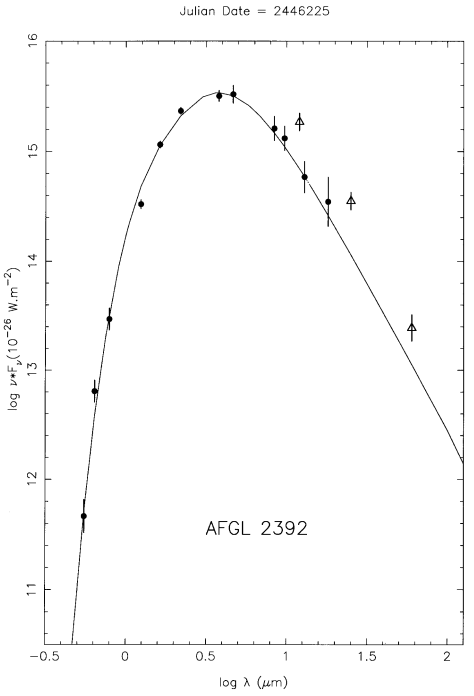

Fig. 13. Same as Fig. 3 for AFGL 2392 (infrared data: JD = 2446220; optical data: JD = 2446225; $\tau_{1\mu m} = 2.4$)

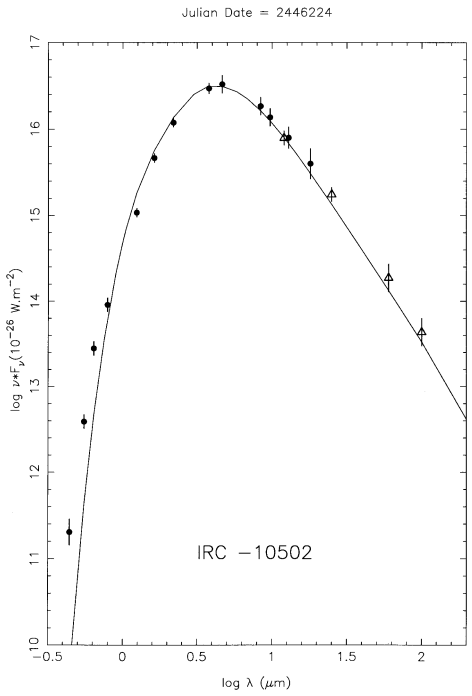

Fig. 12. Same as Fig. 3 for IRC –10502 (infrared data: JD = 2446220; optical data: JD = 2446224; $\tau_{1\mu m} = 3.5$)

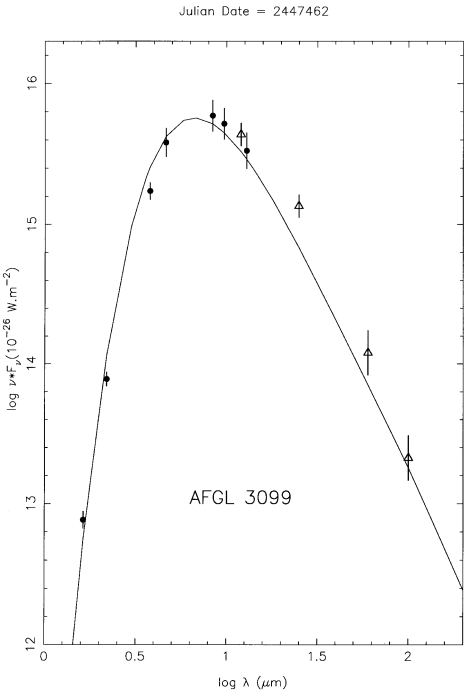

Fig. 14. Same as Fig. 3 for AFGL 3099 (infrared data: JD = 2447462; $\tau_{1\mu m} = 14.0$)

in Table 4. Also, for each object the product $\tau_{1\mu m} \times R_c$ has been maintained constant with phase; again the exact values are given in Table 4.

One should note that, with the method which has been used, the modelling is not strongly constrained when few spectra are available ($n \leq 3$) or when the central source do not undergo large variations. In such cases, the main constraint is provided by the condition $T_c \sim 955$ K. Also when the optical depth is small ($\tau_{1\mu m} \leq 0.3$) the modelling of the CDS becomes sensitive to parameters such as $T_\star$ and is not too reliable.

5. Discussion

5.1. Characteristics of the dust

The numerical models presented here confirm that Jura's law in $\lambda^{-1.3}$ applies widely to the dust around carbon–rich sources. To reproduce the 1–100 μm broad–band spectra, there is no reason to invoke different dust properties from object to object. In that respect, ECSs do not differentiate from optical carbon miras.

The value adopted for T_c, ~ 955 K, is in agreement with the results on the formation of soot in carbon–rich stellar outflows (Cherchneff et al. 1992). On the other hand, it is significantly less than the value of ~ 1300 K obtained by interferometry at 11 μm (Danchi et al. 1990). In Paper II, it has been suggested that heterogeneous condensation could explain this apparent discrepancy. As proposed by Draine (1981), a nucleus would form in the upper part of the stellar atmosphere at a high temperature and grow further away from the central star by accretion. In a carbon–rich environment, SiC would be an attractive candidate for this high–temperature condensate (Gilman 1969). It is undoubtly present in the dust around carbon stars. The 11.3 μm feature is seen in emission in all mass–losing carbon–star spectra, except in the most extreme ECSs where it could be self–absorbed. Furthermore, micrometre–sized SiC grains have been discovered in meteorites. The isotopic anomalies found in these grains show that AGB stars are the most likely sources (Dorschner & Henning 1995). In this context, the model temperature, T_c, would be representative of the accretion/evaporation of a carbonaceous mantle surrounding a SiC core. A difficulty with this interpretation is that the present thermochemical models are unable to predict the nucleation of SiC particles in the normal winds of carbon stars (Sedlmayr 1996). If this situation holds, it might be necessary to consider another composition for the dust nuclei.

Finally, in the modelling presented here, the dust at the inner boundary (R_c) is destroyed when the central star evolves from minimum luminosity to maximum. Such a behavior is supported by the hydrodynamic calculations of Fleischer et al. (1992) which accounts for dust evaporation. In the present work, we do not make a distinction between grain destruction and mantle evaporation. However, from the previous discussion the second option is favored.

5.2. Mass loss rates

With the ST approximation the mass loss rates can be evaluated from:

$$\dot{M} = 16\pi \ (a \ \rho / \ Q_{abs}) \ \tau_{1\mu m} \ R_c \ V_d(R_c)/\delta$$

where a is the grain radius, ρ the dust specific weight, Q_{abs} the absorption efficiency at 1 μm, $V_d(R_c)$ the dust velocity in R_c and δ the dust–to–gas mass ratio. The modelling presented here gives only $\tau_{1\mu m}$ and R_c. We replace this relation by:

$$\dot{M} = C \ \tau_{1\mu m} \ R_c \ V_{exp}$$

where C is a constant and V_{exp}, the gas expansion velocity. By doing so, we implicitely assume that the grain material, the dust–to–gas velocity ratio and the dust–to–gas mass ratio are the same around all sources of the sample.

The numerical value of C can be determined by scaling the relation on IRC +10216. Adopting a mass loss rate of 2.5 10^{-5} $M_\odot$ yr^{-1} for a distance of 200 pc (Truong–Bach et al. 1991):

$$\dot{M} = 0.74 \ 10^{-3} \ \tau_{1\mu m} \ R_c \ V_{exp}$$

with R_c in pc, V_{exp} in km s^{-1} and $\dot{M}$ in $M_\odot$ yr^{-1}. The Truong–Bach et al. result is based on a modelling of the CO radio lines, including the high–J lines which form in the inner CO shell, and is probably the best up–to–date evaluation of the IRC +10216 mass loss rate. The mass loss rates estimated by this method are given in Table 5. When no expansion velocity was available, an arbitrary value of 15 km s^{-1} has been adopted (as well as for AFGL 971, cf Sect. 2.1).

It should be kept in mind that there are some uncertainties in this method. The infrared emissivity and the dust–to–gas ratio are assumed to be always as in IRC +10216. Furthermore, there are simplifications in the modelling (spherical symmetry, constant mass loss rate,...) which may have some consequences on the estimated values.

Nevertheless, apart from R Scl and IRC –20131, the rates given in Table 5 compare well (within a factor 2) with the estimations obtained by Loup et al. (1993) from CO radio measurements. (When discussing mass loss rates, it is useful to remember that an estimation based on CO data scales as the square of the distance, d, whereas an estimation based on IR photometric data scales linearly with d.) For R Scl and IRC –20131, the central sources are not very variable and our modelling is not strongly constrained. Also, there are growing evidences that R Scl has undergone an episode of large mass loss about 10^4 years ago. For this episode, Olofsson et al. (1996) derive a rate $\sim 0.8 \ 10^{-5}$ $M_\odot$ yr^{-1} (d = 420 pc), a value which agrees with the Loup et al. one. On the other hand, they estimate the present–day mass–loss rate to be $\leq 10^{-7}$ $M_\odot$ yr^{-1}; this limit is consistent with our evaluation. R Scl is the only source in our sample for which a large variation in the mass loss rate has been reported in the literature.

For IRSV 1519–5115, on the basis of a model of the spatially resolved CO (1–0) and (2–1) emissions and assuming a distance

Table 5. Mass loss rates

name	adopted exp. velocity $km\,s^{-1}$	$\tau_{1\mu m}\times R_c$ 10^{-3} pc	mass loss rate $10^{-6}\,M_\odot\,yr^{-1}$
R Scl	17.3	0.0052	0.07
R For	20.1	0.0525	0.80
R Lep	18.7	0.0163	0.22
AFGL 799	15.0	0.155	1.70
AFGL 865	16.0	1.450	17.10
IRC –30060	15.0	0.0051	0.06
AFGL 935	13.7	0.280	2.80
AFGL 971	15.0	0.535	5.90
"CRL 1047"	15.0	0.0053	0.06
AFGL 1062	15.0	0.220	2.40
AFGL 1085	23.8	0.326	5.70
IRC –20131	25.5	0.072	1.40
AFGL 1235	20.7	0.310	4.70
IRC +10216	15.0	1.043	11.60
IRAS 11514–5841	15.0	1.912	21.20
IRSV 1204–6417	15.0	0.412	4.60
IRSV 1301–6242	15.0	0.011	0.12
IRSV 1519–5115	22.2	0.565	9.30
IRC +10401	18.2	0.472	6.40
IRC –10502	31.8	0.302	7.10
AFGL 2392	15.0	0.159	1.80
AFGL 3068	14.0	4.660	48.20
AFGL 3099	10.1	1.068	8.00

Note: the values of $\tau_{1\mu m}\times R_c$ are taken from Table 4.

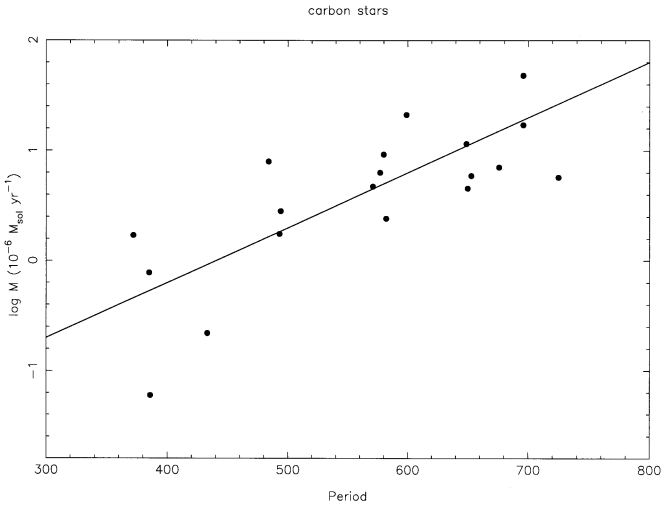

Fig. 15. The mass loss rates as a function of the period for the periodic sources of the sample

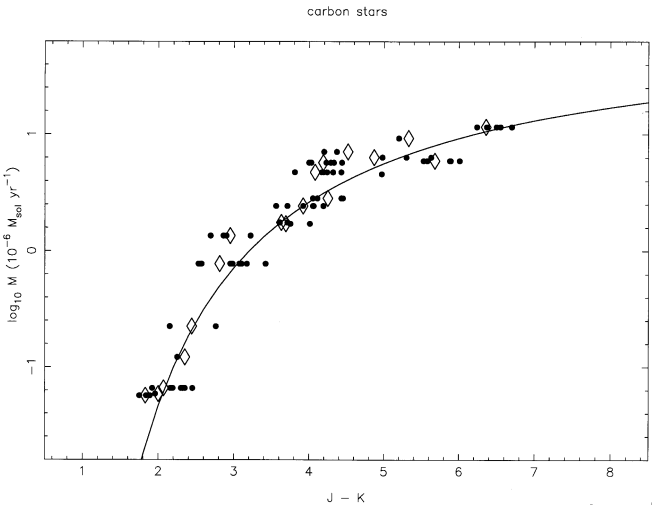

Fig. 16. The mass loss rates as a function of J – K. The curve represents Equ. (1) in Sect. 5.3. The dots corresponds to the individual J – K measurements which have been used in this work, and the empty diamonds to the averages over time of J – K

of 1.2 kpc, Nyman et al. (1993) estimate the mass loss rate to $5\,10^{-5}\,M_\odot\,yr^{-1}$. Adopting d = 1 kpc and by modelling the IR spectrum and high–angular resolution data, Lopez (1994) finds $2.3\,10^{-5}\,M_\odot\,yr^{-1}$. Both determinations are in excellent agreement with the present one obtained for d = 540 pc. Winters et al. (1997), with a consistent time dependent model including a proper treatment of the dust nucleation and of the dynamics, obtain $1.2\,10^{-4}\,M_\odot\,yr^{-1}$ for AFGL 3068 at 1.2 kpc, a factor 2.5 larger than given in Table 5.

Groenewegen (1995) has performed radiative transfer modelling of dust shells around 21 carbon stars. For the 5 objects in common (AFGL 865, AFGL 971, AFGL 1085, IRSV 1519–5115, AFGL 3068), the mass loss rates agree within a factor 2. Finally, Jura & Kleinmann (1989) have estimated, from the IRAS fluxes at 60 μm (Jura 1987), the mass loss rates of nearby AGB stars loosing large amounts of matter. For the 6 objects in common (R For, AFGL 1235, IRC +10216, IRC +10401, IRC –10502 and AFGL 3068) and when corrections are made for distances, the mass loss rates agree within a factor better than 2.

These comparisons with the estimates obtained from different techniques and for objects with a large range of properties indicate that there is no systematic error in our method for evaluating the present–day mass–loss rates of carbon stars.

As already noted in the Introduction, there is a correlation between the period and the mass loss rate (Fig. 15), but this correlation appears loose (at least for the 19 periodic objets in our sample). For instance, one notes for a source like AFGL 1085, with P $\sim$ 725 days, a mass loss rate $\sim 5\,10^{-6}\,M_\odot\,yr^{-1}$, whereas it is found to be $\sim$ 10 times larger for AFGL 3068 which has a similar period (P $\sim$ 700 days). These results are in agreement with those obtained on a larger sample of carbon stars by Claussen et al. (1987, their Fig. 11).

5.3. Near–Infrared colors

Two major surveys of the sky at near–infrared wavelengths have recently been undertaken. With the DEep Near–Infrared Survey (DENIS), it is intended to cover the southern sky in the photometric bands I, J and K. On the other hand, the Two Micron All Sky Survey (2MASS) will cover the whole sky in the bands

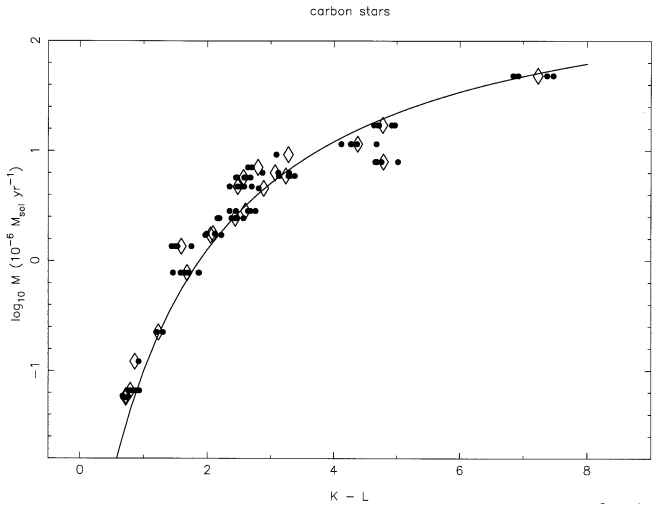

Fig. 17. The mass loss rates as a function of K – L. The curve represents Equ. (2) in Sect. 5.3. The dots corresponds to the individual K – L measurements which have been used in this work, and the empty diamonds to the averages over time of K – L

J, H and K. Many carbon stars will be detected. It is therefore of interest to characterize these objects, for which the distance might not be known a priori, by observed photometric indices and especially by the J – K one which is common to both programmes. In Fig. 16, the mass loss rates are given as a function of J – K. There is a good correlation which can be described with the relation:

$$\log_{10} \dot{M} = -6.0/(J - K - 0.2) + 2.0, \quad (1)$$

with $\dot{M}$ in $10^{-6}\,M_\odot\,yr^{-1}$ and for $2 \leq J-K \leq 7$. There is some scatter around this relation which is partly due to the variability of the sources (they are redder at minimum than at maximum, but the estimates of the mass loss rates stay the same). To illustrate that there is nevertheless an intrinsic scatter, representative points with the average J – K colors (taken from Paper I) are overplotted as diamonds.

The correlation is still better with the near–infrared index K – L (Fig. 17):

$$\log_{10} \dot{M} = -9.0/(K - L + 1.4) + 2.75, \quad (2)$$

for $1 \leq K-L \leq 8$. As explained in Sect. 4.2, the K – L color is less sensitive to the stellar photospheric parameters than the J – K. Also, the amplitudes of the light curves in K – L are smaller than in J – K. For AFGL 3099 ($K-L \sim 4.8$, $\log_{10} \dot{M} \sim 0.9$), the data points stand out apart from the others. The expansion velocity ($10\,km\,s^{-1}$) is surprisingly low for an object with a large optical depth ($\tau_{1\mu m} \sim 12$). With an expansion velocity $\sim 15\,km\,s^{-1}$, the AFGL 3099 data would fit better with the others.

Using the Jura (1987) method, Epchtein et al. (1990) have derived the mass loss rates of ~ 190 carbon stars for which they had obtained near–infrared photometry. They adopt distances based on an average carbon star luminosity ($7000\,L_\odot$). The results presented in their Fig. 14 are in good statistical agreement with relation (2).

6. Conclusion

The 23 carbon–rich sources studied in the present work can be modelled in spherical geometry with an opacity law $\propto \lambda^{-1.3}$. The examination of sources with moderate optical depth ($\tau_{1\mu m} \sim 1$) supports that dust is accelerated from its formation site, at a few 10^{14} cm from the central star, and on a distance of $\sim 10^{15}$ cm.

The modelling presented here supports the suggestion presented in Paper II that dust grains around carbon stars might be made of a high–temperature condensate core (formed at ≥ 1300 K) and of a hydrogeneous carbonaceous mantle condensing/evaporating at ~ 950 K. It was also suggested that this core could be made of SiC. However, this suggestion requires more theoretical developments on the formation of solid SiC.

Estimates of the mass loss rates which are consistent within a factor 2.5 with those obtained with other methods are derived from the modelling. The near infrared colors are well correlated with the mass loss rate, so that it should be possible to evaluate the contribution of carbon stars to the replenishment of the Interstellar Medium from the data obtained through surveys such as DENIS and 2MASS.

Acknowledgements. I am grateful to A. Fleischer, E. Sedlmayr and J.–M. Winters for enlightening discussions, and to M. Jura, J. Lequeux, B. Lopez and N. Mauron for a careful reading of the original manuscript.

References

Allen D.A., Hyland A.R., Longmore A.J., et al., 1977, ApJ 217, 108
Barthès D., Chenevez J., Mattei J.A., 1996, AJ 111, 2391
Begemann B., Dorschner J., Henning T., Mutschke H., Thamm E., 1994, ApJ 423, L71
Cherchneff I., Barker J.R., Tielens A.G.G.M., 1992, ApJ 401, 269
Claussen M.J., Kleinmann S.G., Joyce R.R., Jura M., 1987, ApJS 65, 385
Cohen M., 1979, MNRAS 186, 837
Danchi W.C., Bester M., Degiacomi C.G., McCullough P.R., Townes C.H., 1990, ApJ 359, L59
Day K.L., 1974, ApJ 192, L15
DeGioia–Eastwood K., Hackwell J.A., Grasdalen G.L., Gehrz R.D., 1981, ApJ 245, L75
Dominik C., Gail H.–P., Sedlmayr E., Winters J.–M., 1990, A&A 240, 365
Dorschner J., Henning T., 1995, A&AR 6, 271
Draine B.T., 1981, in "Physical Processes in Red Giants", ed. by Iben and Renzini, p. 317
Epchtein N., Le Bertre T., Lépine J.R.D., 1990, A&A 227, 82
Feast M.W., Whitelock P.A., Catchpole R.M., Roberts G., Overbeek M.D., 1984, MNRAS 211, 331
Fleischer A.J., Gauger A., Sedlmayr E., 1992, A&A 266, 321
Gilman R.C., 1969, ApJ 155, L185
Goebel J.H., Moseley S.H., 1985, ApJ 290, L35
Groenewegen M.A.T., 1995, A&A 293, 463
Groenewegen M.A.T., Whitelock P.A., 1996, MNRAS 281, 1347
Groesbeck T.D., Phillips T.G., Blake G.A., 1994, ApJS 94, 147
IRAS Science Team, 1988, IRAS Catalogs and Atlases, NASA RP–1190
Jura M., 1983, ApJ 267, 647
Jura M., 1986, ApJ 303, 327

Jura M., 1987, ApJ 313, 743
Jura M., Kleinmann S.G., 1989, ApJ 341, 359
Kwok S., 1975, ApJ 198, 583
Le Bertre T., 1987, A&A 176, 107
Le Bertre T., 1988a, A&A 190, 79
Le Bertre T., 1988b, A&A 203, 85 (Paper III)
Le Bertre T., 1990, A&A 236, 472
Le Bertre T., 1992, A&AS 94, 377 (Paper I)
Le Bertre T., Gougeon S., Le Sidaner P., 1995, A&A 299, 791 (Paper II)
Le Sidaner P., Le Bertre T., 1993, A&A 278, 167
Le Sidaner P., Le Bertre T., 1996, A&A 314, 896
Leung C.M., 1975, ApJ 199, 340
Lopez B., 1994, PhD thesis, University of Nice–Sophia Antipolis
Lopez B., Perrier C., Mékarnia D., Lefèvre J., Gay J., 1993, A&A 270, 462
Loup C., Forveille T., Omont A., Paul J.F., 1993, A&AS 99, 291
Nyman L.–Å., Olofsson H., Johansson L.E.B., et al., 1993, A&A 269, 377
Nyman L.–Å., Thaddeus P., Bronfman L., Cohen R.S., 1987, ApJ 314, 374
Ohnaka K., Tsuji T., 1996, A&A 310, 933
Olofsson H., Bergman P., Eriksson K., Gustafsson B., 1996, A&A 311, 587
Rowan–Robinson M., Lock T.D., Walker D.W., Harris S., 1986, MNRAS 222, 273
Salpeter E.E., 1974, ApJ 193, 579
Schutte W.A., Tielens A.G.G.M., 1989, ApJ 343, 369
Sedlmayr E., 1996, personal communication
Tielens A.G.G.M., 1983, ApJ 271, 702
Treffers R., Cohen M., 1974, ApJ 188, 545
Truong–Bach, Morris D., Nguyen–Q–Rieu, 1991, A&A 249, 435
Whitelock P.A., Menzies J., Feast M.W., et al., 1994, MNRAS 267, 711
Winters J.M., Dominik C., Sedlmayr E., 1994a, A&A 288, 255
Winters J.M., Fleischer A.J., Gauger A., Sedlmayr E., 1994b, A&A 290, 623
Winters J.M., Fleischer A.J., Le Bertre T., Sedlmayr E., 1997, A&A, in press
Zuckerman B., Dyck H.M., 1986, ApJ 304, 394

This article was processed by the author using Springer-Verlag LaTeX A&A style file *L-AA* version 3.